Monatshefte für Chemie - Chemical Monthly (2022) 153:507–515
https://doi.org/10.1007/s00706-022-02919-7

ORIGINAL PAPER

Spectroscopic analysis of 2-(5-mercapto-1,3,4-oxadiazol-2-yl)-6-methylquinolin-4-ol binding to blood plasma albumin

Karine R. Grigoryan[1] · Hasmik A. Shilajyan[1] · Ashkhen Zatikyan[1] · Iskuhi Aleksanyan[2] · Lilit Hambardzumyan[2]

Received: 13 August 2021 / Accepted: 25 April 2022 / Published online: 9 May 2022

Abstract

Binding of 2-(5-mercapto-1,3,4-oxadiazol-2-yl)-6-methylquinolin-4-ol (C1), a biologically active substance, to bovine blood plasma albumin (BSA) at 293, 298, and 303 K was studied using fluorescence (steady state, synchronous, excitation/emission matrix) and FT-IR spectroscopy methods. The experimental results showed that C1 causes fluorescence quenching of BSA through both static and dynamic quenching mechanisms. The thermodynamic parameters, enthalpy and entropy change, for the static quenching were calculated to be − 35.73 kJ mol^{-1} and − 35.34 J mol^{-1} K^{-1}, which indicated that hydrogen bonding and van der Waals interactions were the predominant intermolecular forces regulating C1–BSA interactions. Distance between donor and acceptor (2.14, 2.26, and 2.30 nm) depending on the temperature, obtained from intrinsic Förster resonance energy transfer calculations, revealed the static quenching mechanism of BSA fluorescence in 0–3.0 × 10^{-5} mol/dm^3 concentration range of C1. The micro-environmental and conformational changes in BSA structure, established by synchronous, excitation/emission matrices and FT-IR spectra showed the changes in the BSA secondary structure.

Graphical abstract

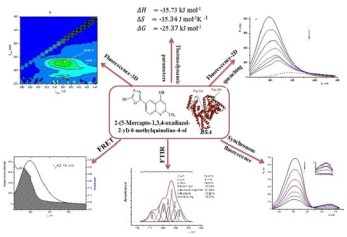

Keywords Binding · Bovine serum albumin · Fluorescence · IR spectroscopy · Quinoline

Introduction

Quinoline-containing pharmacophore compounds are widely used in the design of drugs exhibiting antifungal, antibacterial and antiprotozoic, antiasthmatic, as well as antineoplastic properties [1–4]. Some quinoline derivatives show an antiplatelet activity as well [5, 6]. The effectiveness of some quinoline drugs, chloroquine and hydroxychloroquine, towards COVID-19 in the in vitro experiments showed that they could inhibit the duplication of the SARS-CoV-2 virus [7]. Quinoline is recognized as a privileged scaffold/substructure in cancer and antimicrobial drugs [8]. Derivatives of quinolines, such as hydroxyqunolines, also exhibit biological activity; alkenyl side chain of hydroxyquinolines/hydroxyquinolones can have an impact on antimicrobial properties due to hydrophobic interactions at a binding pocket of transporting proteins [9]. *N*-Methyl-2-alkenyl-4-quinolones are inhibitors of mycobacterial and staphylococcal growth, and show MurE ligase inhibition. The important feature of hydroxyquinolines is that they can exist in keto and enol

✉ Karine R. Grigoryan
kara@ysu.am

[1] Laboratory of Physical Chemistry, Chemistry Research Center, YSU, Yerevan, Armenia

[2] Laboratory of Organic Chemistry, Chemistry Research Center, YSU, Yerevan, Armenia

tautomeric forms; moreover, they can form dimers, which possess unique properties [10]. Penetration of quinoline/quinolone dimers into the red blood cell is unlikely due to steric bulk that can affect the destabilization of red cell membrane inducing hemolysis, which is the main cause of toxicity. Moreover, quinoline/quinolone dimers may have dual-action mechanism, and consequently increase the antiplasmodial and antimalarial activities [11].

In the field of drug discovery and pharmaceutical sciences, binding of various drugs to plasma protein like serum albumin is of special interest since drug–albumin binding interaction decreases bioavailability and increases the in vivo half-life of the drug. On the other hand, one aspect in drug design is crucial from the point of view how to find perfect privileged structure (structure–activity relationship). Finding out the transport mechanism of these molecules can promote solving such problems. The spectrofluorometric analysis of target molecule to serum albumin help to deepen enlightenment of reactivity features which is useful in designing optimized drugs [12].

Serum albumin is the most abundant plasma carrier protein, which is responsible for transporting and distributing many endogenous and exogenous substances [13–15]. Human serum albumin (HSA) and bovine serum albumin (BSA) are commonly used as model proteins in biopharmaceutical studies. These proteins are synthesized by the parenchymal cells of the liver and exported as a non-glycosylated protein. HSA and BSA display approximately similar structure and sequence of amino acid residues [16]. From the spectroscopic point of view, one of the main differences between the two proteins is that HSA has only one tryptophan (Trp) residue (Trp-214), whereas BSA is characterized by two Trp residues Trp-134 and Trp-214 located in the subdomains IB and IA of BSA, respectively. Trp-214 is buried in a hydrophobic pocket of protein, very close to the second helix of the first domain of the albumin molecule, whereas Trp-134 is considered to be more exposed to solvent, and is very sensitive to any change in microenvironment polarity [17]. BSA possesses absorption (UV/Vis) and emission (fluorescence) property due to the existence of aromatic amino acids phenylalanine (Phe), tyrosine (Tyr), and Trp residues. By monitoring the intrinsic fluorescence change of BSA, binding affinities (binding mechanism, binding mode, binding constants, binding sites, intermolecular distance, etc.) of small molecules can be determined.

The present study is focused on the fluorescence and FT-IR analysis of 2-(5-mercapto-1,3,4-oxadiazol-2-yl)-6-methylquinolin-4-ol (C1) binding peculiarities to BSA. Molecular structure of C1 is presented in Fig. 1. This work may provide some valuable information for the quinoline scaffold design and can be helpful for clarifying the toxicity and dynamics of C1.

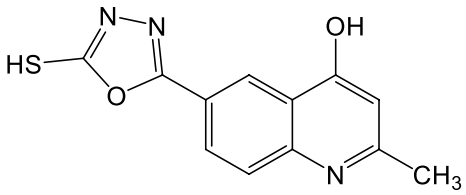

Fig. 1 Structure of 2-(5-mercapto-1,3,4-oxadiazol-2-yl)-6-methylquinolin-4-ol

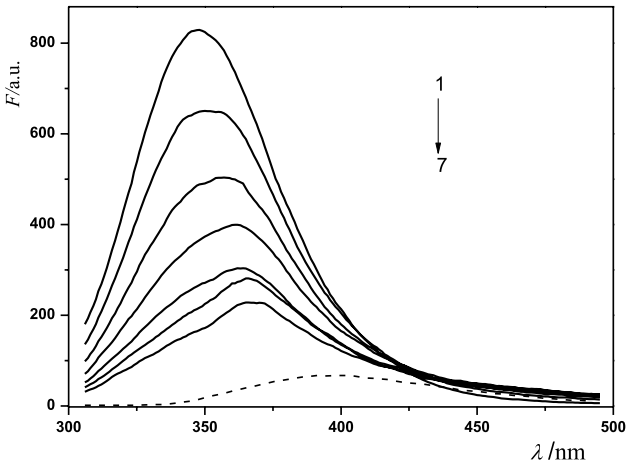

Fig. 2 Fluorescence spectra of BSA in the presence of various concentrations of C1 at $T=293$ K. (BSA) $=6.0\times10^{-6}$ mol/dm^3, 1–7 (C1) $=0\div6.0\times10^{-5}$ mol/dm^3. Dash curve shows the emission spectrum of C1 only at (C1) $=1.0\times10^{-5}$/mol/dm^3

Results and discussion

Fluorescence quenching mechanism analysis of BSA in the presence of C1

The intrinsic fluorescence of BSA is mainly due to Trp residues, because Phe has a very low quantum yield and the fluorescence of Tyr is almost totally quenched if it is ionized or near an amino or carboxyl group, or a resonance energy transfer can occur from Tyr to Trp residues [18]. When a small molecule interacts with BSA, the changes of fluorescence parameters are observed. The fluorescence spectra of BSA in the presence of various concentrations of C1 at 293 K are presented in Fig. 2.

Fluorescence spectrum of BSA is characterized by a strong fluorescence emission band at about 348 nm ($\lambda_{ex}=$ 280 nm), while C1 fluorescence is negligible under the experimental conditions ($\Phi_f=0.027$) [19]. Upon addition of C1 a decrease in fluorescence intensity of BSA with a red shift is observed, indicating on the interaction between BSA and C1 molecules, and changes in the chromophore microenvironment polarity. At the higher concentrations of

C1 "Gaussian-like" shape of the BSA emission spectrum changes into a "strange-pointed" shape, which indicates some absorption phenomena for excitation and/or emission light.

As it is mentioned in [20–24], quenching of a macromolecule fluorescence caused by the addition of a compound to a solution may be a result of inner-filter effect, ground-state complex formation, collisional quenching, excited-state reactions, fluorescence resonance energy transfer (Förster theory), or molecular rearrangements. Quenching data are usually presented as a plot of F_0/F versus $[Q]$ (Stern–Volmer plot, Eq. (1)) because F_0/F is expected to be linearly dependent upon the quencher concentration.

$$\frac{F_0}{F} = 1 + k_q\tau_0[Q] = 1 + K_D[Q], \tag{1}$$

where F_0 and F represent the fluorescence intensities of fluorophore in the absence and presence of quencher, respectively, kq is the bimolecular quenching rate constant, τ_0 is the average lifetime of the fluorophore in the absence of a quencher, K_D is Stern–Volmer quenching constant, and $[Q]$ is the concentration of the quencher.

A linear Stern–Volmer plot generally indicates homogeneous quenching (static or dynamic). The dynamic/static mechanism of quenching can be distinguished from the differing effect of temperature or viscosity on the Stern–Volmer constant values. Static quenching is related to the formation of non-fluorescent complex between the fluorophore and the quencher in the ground state; science higher temperatures decrease the stability of complexes, whereas dynamic quenching depends on diffusion of fluorophore and higher temperatures, result larger diffusion coefficients and the constants are expected to increase [17]. Fluorescence spectra of BSA in the presence of C1 and the Stern–Volmer plots at different temperatures are presented in Fig. 3.

The Stern–Volmer plots deviate from linearity with an upward curvature, concave towards the F_0/F-axis indicating combined/competitive fluorescence quenching. This means that fluorophore may be quenched both by collisional (in the excited state) and by complex formation (in the ground state) with the same quencher. In this case, the modified Stern–Volmer equation Eq. (2) could be used to determine dynamic (K_D) and static (K_S quenching constants:

$$\frac{F_0}{F} = \big(1 + K_D[Q]\big)\big(1 + K_s[Q]\big). \tag{2}$$

Linear relationship of the Stern–Volmer plot is observed in the concentration range of C1 from 0 to 3.00×10^{-5} mol/dm^3, where "Gaussian-like" shape of the BSA emission spectra are observed at $\lambda_{max} = 348$ nm with a red shift (13 nm). The K_S values, calculated from the slope of curves in inset, and k_q are listed in Table 1. The

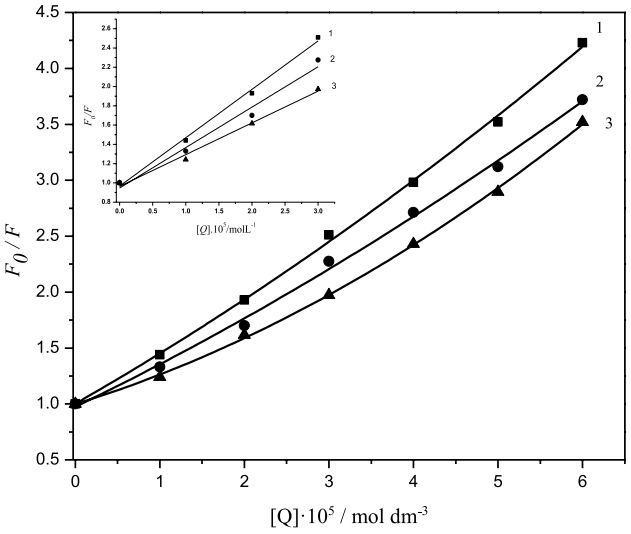

Fig. 3 Stern–Volmer plots for BSA–C1 at different temperatures. 1. 293, 2. 298, 3. 303 K. Inset: linear relationship of the Stern–Volmer plot [concentration range of C1 from 0 to 3.00×10^{-5} mol/dm^3, (BSA) = 6.0×10^{-6} mol/dm^3]

Table 1 Stern–Volmer quenching constant (K_S) and the bimolecular quenching rate constant k_q for the interaction of C1 with BSA at different temperatures

T/K	$10^4(K_S \pm SD^a)/dm^3$ mol^{-1}	$10^{12}k_q/dm^3mol^{-1}s^{-1}$	R^b
293	5.03 ± 0.01	5.03	0.99803
298	4.37 ± 0.03	4.37	0.99083
303	3.59 ± 0.02	3.59	0.99597

[a]SD is the standard deviation for the K_S values

[b]R is the correlation coefficient

results show that the Stern–Volmer quenching constant is inversely correlated with temperature and the k_q value is larger than the limiting diffusion collision quenching rate constant (2.09×10^{10} dm^3 mol^{-1} s^{-1}) which indicates that static quenching is involved in BSA-C1 interaction as well.

Thermodynamic parameters and binding forces

The thermodynamic parameters: enthalpy change (ΔH), entropy change (ΔS), and Gibbs energy change (ΔG) are the main quantities used to determine the binding mode. Based on the signs and magnitudes of ΔH and ΔS, Ross and Subramanian have characterized interaction forces between small organic molecules and proteins as reversible, noncovalent binding (hydrophobic forces, hydrogen bond, van der Waals forces, and electrostatic interactions) [25]. The type of binding forces was determined by the relationships of the

thermodynamic parameters (ΔH, ΔS, and ΔG) according to the equations:

$$\ln K_b = -\frac{\Delta H}{RT} + \frac{\Delta S}{R}, \tag{3}$$

$$\Delta G = \Delta H - T\Delta S = -RT \ln K_b, \tag{4}$$

where K_b corresponds to the binding constant and R is the gas constant.$\triangle H$ and $\triangle S$ could be determined from Van't Hoff plot. K_b and the number of binding sites (n) were determined according to the Eq. (5) [26], based on the BSA fluorescence quenching data by C1.

$$\lg \frac{F_0 - F}{F} = \lg K_b + n \lg [Q], \tag{5}$$

where F_0 and F are the fluorescence intensities of BSA in the absence and presence of C1, respectively; K_b is the binding constant, n is the number of binding sites, and $[Q]$ is the concentration of quencher. The plot of $lg[(F_0 - F)/F]$ versus lg[Q] and Van't Hoff plot for the binding of C1 to BSA is presented in Fig. 4, (Table 2)

The negative values of ΔG show that the binding process proceeds spontaneously. The negative values of ΔH and ΔS show that the stability of the BSA–C1 complex is mainly specified by hydrogen bond formation and van der Waals forces interactions. According to the classification of Trp residues based on discriminant analysis, BSA belongs to Class III ($\lambda_{max} > 347.0 \pm 3.1$ nm), possessing spectra almost coinciding in position and shape with those of free aqueous Trp [27]. The red shift of Trp $\lambda_{\max}$ and no changes in the shape of the band confirm H-bond formation between BSA and C1.

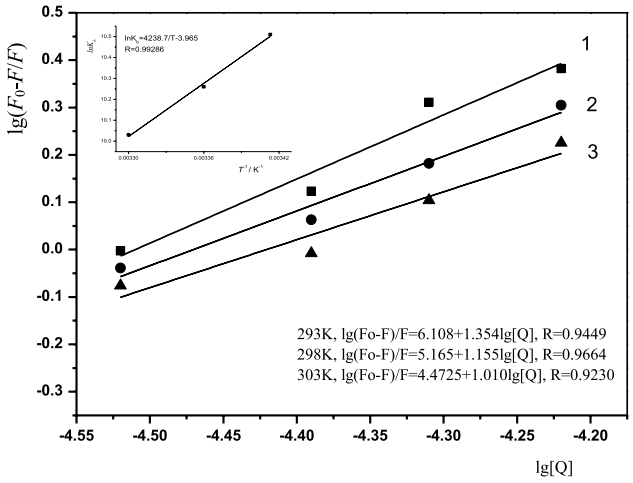

Fig. 4 $lg[(F_0 - F)/F]$ versus lg[Q]. 1. 293, 2. 298, 3. 303 K. Inset: Van't Hoff plot for the binding of C1 to BSA

Energy transfer

Förster resonance energy transfer (FRET) is a long-range (1–10 nm) non-radiative energy transfer process between a donor fluorophore (in the excited state) and an acceptor molecule (in the ground state). It is a powerful technique to study specific and dynamic processes in biomolecules. Intrinsic Förster resonance energy transfer (iFRET) utilizes the intrinsic fluorescence of Trp in conjunction with target-specific fluorescent probes as FRET donors and acceptors, respectively, for real time detection of native proteins [28]. The binding distance between BSA and C1 is calculated using iFRET. The efficiency of energy transfer E is calculated using the equation:

$$E = 1 - \frac{F}{F_0} = \frac{R_0^6}{R_0^6 + r^6}, \tag{6}$$

where E is the energy transfer efficiency, F_0 and F are the fluorescence intensities of BSA in the absence and presence of quencher, respectively; r is the distance between the donor and the acceptor, R_0 is the Förster radius, when the energy transfer efficiency is 50% and can be calculated by the following equation:

$$R_0^6 = 8.79 \times 10^{-25} \kappa^2 n^{-4} \phi J, \tag{7}$$

where k^2 is the spatial orientation factor ($k^2 = 2/3$); n is the refractive index (1.336); ϕ is the fluorescence quantum yield of the donor (0.15) [18]; J is the overlap integral of the donor fluorescence spectrum and the acceptor absorption spectrum.

$$J = \frac{\sum F(\lambda)\varepsilon(\lambda)\lambda^4 \Delta\lambda}{F(\lambda)\Delta\lambda}, \tag{8}$$

where $F(\lambda)$ is the fluorescence intensity of the donor at wavelength λ, ε (λ) is the molar extinction coefficient of acceptor at wavelength λ. Using Eqs. (6)–(8), the overlap integral (Fig. 5), the energy transfer efficiency, the Förster's

Table 2 Binding constant, thermodynamic parameters and the number of the binding sites at different temperatures

T/K	10^4 K_b/dm^3 mol^{-1}	ΔH/kJ mol^{-1}	ΔS/J mol^{-1} K^{-1}	ΔG/kJ mol^{-1}	n
293	3.67 ± 0.19	− 35.73 ± 0.25	− 35.34 ± 0.85	− 25.37 ± 0.25	1.35 ± 0.18
298	2.85 ± 0.15			− 25.20 ± 0.25	1.15 ± 0.12
303	2.27 ± 0.21			− 25.02 ± 0.25	1.01 ± 0.16

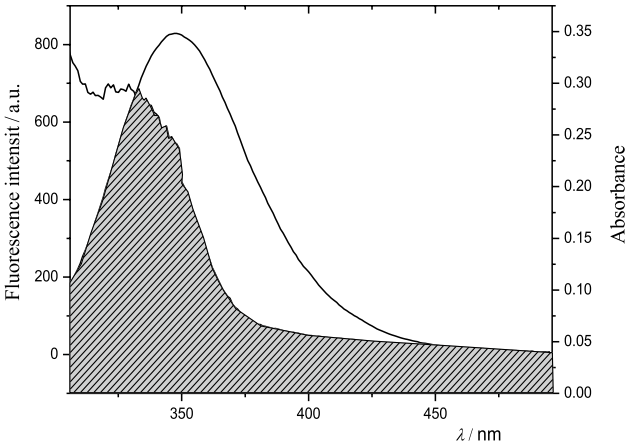

Fig. 5 Spectral overlap of fluorescence emission spectrum of BSA with UV/Vis absorption spectrum of C1. (BSA) = 6.0×10^{-6} mol/dm^3, (C1) = 1.0×10^{-5} mol/dm^3, $T = 293$ K

Table 3 The values of the overlap integral (J), the energy transfer efficiency (E), the Förster radius (R_0) and the distance between BSA and C1 (r)

T/K	10^{-12} J/cm^3 dm^3 mol^{-1} ($\pm 0.008 \times 10^{-12}$)	E (± 0.00019)	R_0/nm (± 0.00009)	r/nm (± 0.0084)
293	2.68	0.226	4.5525	2.14
298	2.69	0.162	4.5533	2.26
303	2.69	0.140	4.5534	2.30

radius and the distance between the donor and the acceptor were calculated and given in Table 3.

The distance between Trp-214 and C1 is less than 8 nm, which suggests that the energy transfer from BSA to C1 occurred with high probability. With the increasing temperature, the distance between D–A becomes larger revealing the static quenching mechanism of BSA fluorescence in mentioned concentration range of C1.

Synchronous fluorescence spectral analysis

Synchronous fluorescence method involves measuring the fluorescence spectrum through the simultaneous scanning of the excitation and the emission monochromators of a spectrofluorometer with a fixed wavelength difference. Synchronous fluorescence spectra of BSA (Fig. 6) provide an information for the Tyr and Trp residues when the scanning interval ($\Delta\lambda$) is fixed at 15 and 60 nm, respectively [29]. Synchronous spectra with $\Delta\lambda = 15$ nm effectively enhance the Tyr component with respect to Trp emission.

Synchronous fluorescence spectra of BSA ($\Delta\lambda = 15$ nm) are characterized by an emission peak at $\lambda = 287$ nm. With the addition of C1 a decrease in the fluorescence intensity of BSA is observed. Moreover, there is no significant shift of the maximum emission wavelength. As synchronous fluorescence spectra with $\Delta\lambda = 15$ nm can isolate contribution of Tyr emission only for proteins with water-exposed Trp residues [30], so obtained results may relate only to the Trp-134 residue in BSA structure. In the case of $\Delta\lambda = 60$ nm, the synchronous fluorescence spectra of BSA are characterized by 2 emission peaks: one at $\lambda = 282$ and second $\lambda = 325$ nm. At higher concentrations of C1 a clear iso-emissive point appears at 325 nm, initially as a shoulder and afterwards as a band, reflecting an equilibrium between two distinct emitting species and/or nonradiative energy transfer between aromatic amino acid residues of protein. The ratios of synchronous fluorescence quenching (RSFQ) could be determined from the following equation:

$$\mathrm{RSFQ} = 1 - F/F_0, \tag{9}$$

where F and F_0 are the synchronous fluorescence intensities of BSA in the presence and the absence of C1, respectively. It was obvious from Fig. 6 that the RSFQ for $\Delta\lambda = 15$ nm (RSFQ = 0.8707) was slightly higher than the RSFQ for $\Delta\lambda = 60$ nm (RSFQ = 0.8044), suggesting that C1 was more accessible to Tyr than to Trp residue.

Three-dimensional fluorescence spectral analysis

Among fluorescence spectroscopy methods, excitation–emission matrix method, also called three-dimensional (3D) fluorescence, is widely used to analyze multiple fluorophores with overlapping spectra. The outstanding advantage of three-dimensional fluorescence spectra is that the information regarding the fluorescence characteristics can be entirely acquired by simultaneously changing the excitation and emission wavelengths. The maximum emission wavelength and the fluorescence intensity of the residues have a close relation to the polarity of their microenvironment [31, 32]. The 3D spectra contour maps for protein as well as for BSA-C1 are shown in Fig. 7 and the corresponding characteristic parameters are listed in Table 4.

Three-dimensional spectra of BSA are characterized by two peaks: peak 1 at approximately $\lambda_{ex}/\lambda_{em} = 230/349$ nm/nm and peak 2 at $\lambda_{ex}/\lambda_{em} = 280/349$ nm/nm. Peak 1 often attributed to protein "backbone fluorescence". Actually, it originates from the fluorescence of aromatic residues and peptide backbone does not contribute at all to protein fluorescence. The peak 1 located at $\lambda_{ex}/\lambda_{em} = 230/349$ nm/nm is simply due to the excitation of the second excited state of the aromatic residues which then emit from their lowest excited state, according to Kasha's rule [33]. Peak 2 corresponds to emission of the aromatic amino acids Trp and

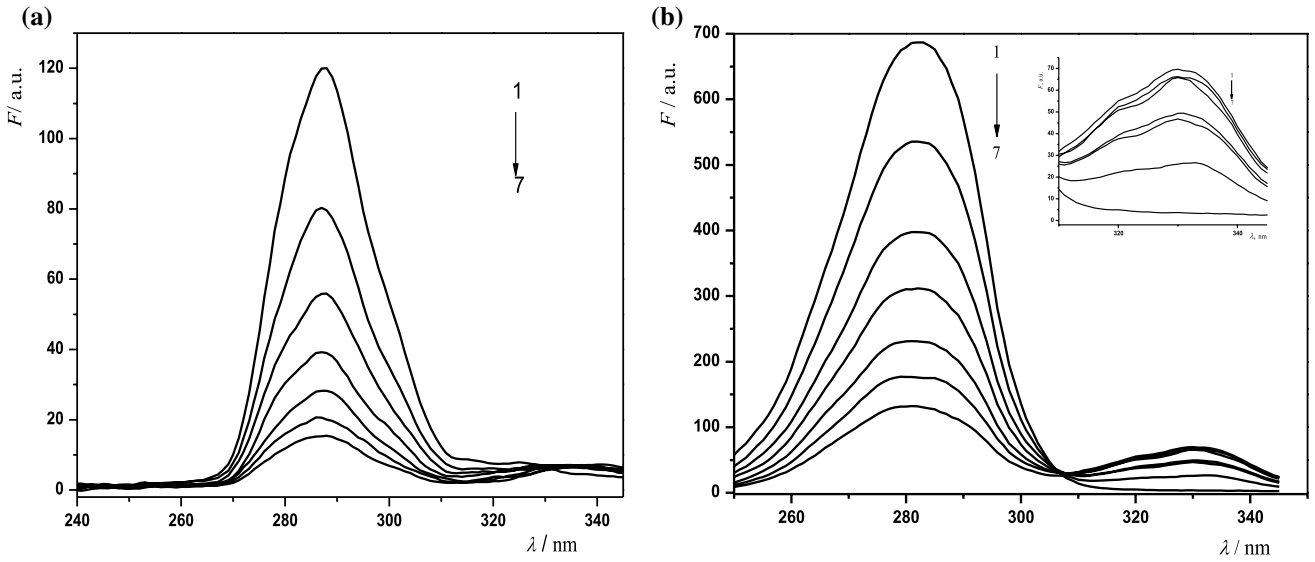

Fig. 6 Synchronous fluorescence spectra of BSA–C1. (BSA) = 6.0×10^{-6} mol/dm^3, 1–7 (C1) = $0 \div 6.0 \times 10^{-5}$ mol/dm^3, **a** $\Delta\lambda = 15$ nm, **b** $\Delta\lambda = 60$ nm, $T = 293$ K

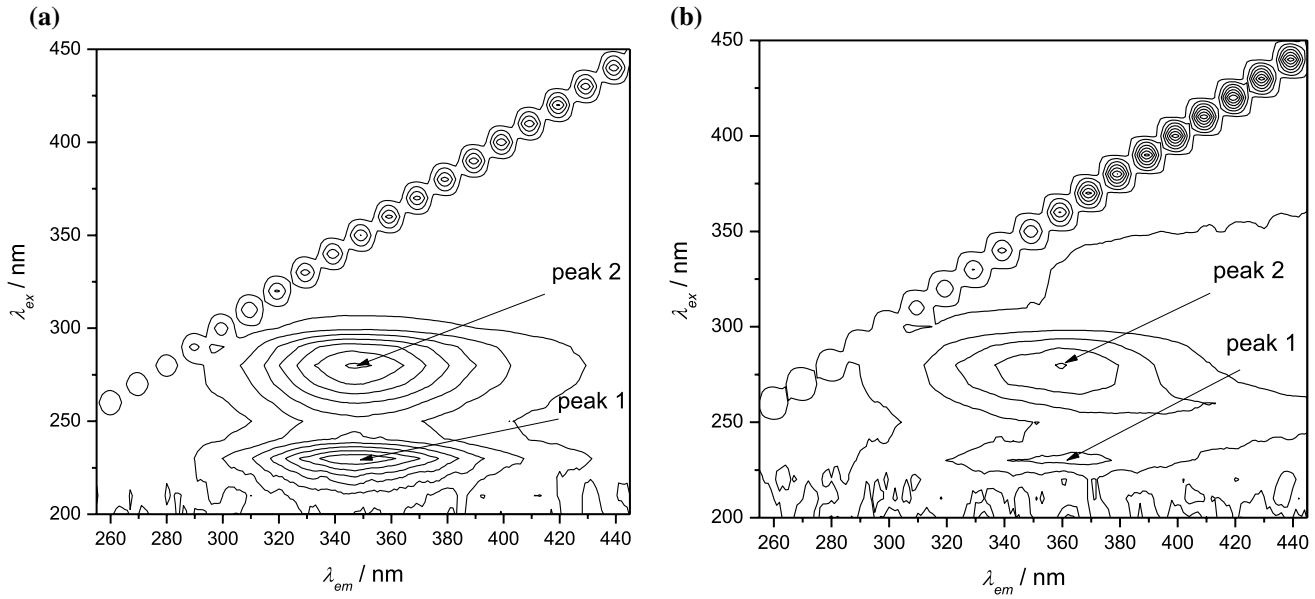

Fig. 7 The 3D spectral contour maps for BSA (**a**) and BSA–C1 (**b**). (BSA) = 6.0×10^{-6} mol/dm^3, (C1) = 3.0×10^{-5} mol/dm^3

Tyr residues. Despite the fact that the quantum yields of Tyr and Trp fluorescence are comparable (0.14 and 0.13, respectively) [18]; however, Tyr fluorescence in proteins is usually rather weak, because of Förster's resonance energy transfer (FRET) from Tyr to Trp residues. Peak (a) is the Rayleigh scattering peak ($\lambda_{ex}/\lambda_{em}$). Addition of C1 resulted in 2–4 times reduction of both peaks (Fig. 7b) and λ_{max} shift to the region of longer wavelengths, suggesting the microenvironmental and conformational changes of BSA. Formation of BSA–C1 complex affects the Rayleigh scattering increasing its intensity approximately 2–3 times. Peak 2, which mainly reveals the spectral characteristic of Trp and Tyr residues, is related to changes in the conformation of the peptide backbone, associated with the helix-coil transformation. Therefore, FT-IR analyses were performed to elucidate the changes in the secondary structure of BSA.

Table 4 The 3D fluorescence spectra characteristics of C1—BSA at different temperatures

10^{-5} [C1]/ mol/dm^3	Peak1		Peak 2		Rayleigh scattering
	$\lambda_{ex}/\lambda_{em}$/ nm/nm	F/ a.u	$\lambda_{ex}/\lambda_{em}$/ nm/nm	F/ a. u	$\lambda_{ex}/\lambda_{em} \rightarrow \lambda_{ex}/\lambda_{em}$ 260/260 → 440/440/ nm/nm
					F/a. u
293 K					
0	230/349	168.8	280/349	149.6	32.6 → 92.4
1.0	230/352	99.1	280/352	109.0	22.7 → 87.1
3.0	230/364	41.9	280/360	69.8	13.3 → 106.8
6.0	–	–	280/370	38.3	8.1 → 89.5
298 K					
0	230/347	190.4	280/347	130.7	38.2 → 136.9
1.0	230/350	109.9	280/350	100.7	31.9 → 130.6
3.0	230/357	50.3	280/357	60.6	23.9 → 157.8
6.0	–	–	280/365	35.8	8.9 → 122.2
303 K					
0	230/348	165.4	280/348	118.4	29.7 → 98.9
1.0	230/349	94.3	280/349	95.8	23.9 → 101.5
3.0	230/361	53.1	280/361	61.3	19.6 → 131.5
6.0	–	–	280/372	32.6	9.3 → 116.4

FT-IR spectroscopy studies

FT-IR is widely used for the quantitative analysis of the secondary structure of proteins. FT-IR spectrum of a protein exhibits a number of amide bands, which represent different vibrational modes of the peptide moiety. In all amide modes of the peptide group, amide I bands in the 1600–1700 cm^{-1} region (mainly C=O stretch) and amide II bands in the 1500–1600 cm^{-1} region (C–N stretch coupled with N–H bending mode) are usually used for the analysis of the secondary structure of the protein [34, 35]. Amide I band of BSA in physiological solution is characterized by two peaks at 1648 and 1631 cm^{-1} and amide II band is characterized by one peak at 1544 cm^{-1} (Fig. 8). The peak positions of amide I band at 1648 cm^{-1} were shifted to 1665 cm^{-1} and the intensity of peak reduced upon the addition of C1 to BSA solution and peak at 1631 cm^{-1} was shifted 1635 cm^{-1} and a new peak appeared at 1703 cm^{-1}. The peak position of amide II band was not changed. The analysis of the secondary structure of BSA and BSA–C1 complex (Fig. 9) is carried out for the absorption band of amide I (1700–1600 cm^{-1}) by deconvolution of this band into separate components.

The curve fitting of amide I stretching region for BSA results in 5 components, which describe BSA secondary structure elements: β-turns (1671, 1639, and 1628 cm^{-1}), α–helixes (1651 cm^{-1}), and intermolecular β-sheet (1615 cm^{-1}). A binding interaction of C1 with BSA results in changes in frequencies and band areas. A new component at 1700 cm^{-1} is observed which could be attributed to the β-turn forms. These results indicated that BSA–C1 complex formation caused the rearrangement of the polypeptide carbonyl hydrogen-bonded species and finally led to the reduction of the protein helical structure.

Conclusion

This study presents the binding interaction and mechanism of C1 with BSA using fluorescence and FT-IR spectroscopy methods. The analysis of the steady-state fluorescence quenching data at several temperatures and the Stern–Volmer plots indicated a combined/competitive quenching mechanism in the presence of C1. The predominance of hydrogen bond and van der Waals forces in the C1 interaction with BSA was revealed from the thermodynamic studies and the distance (about 2.14 nm) between Trp-214 residue of BSA and C1 was determined using FRET. The results of synchronous spectroscopy fluorescence suggested that Trp residues have more pronounced contribution in the BSA intrinsic fluorescence quenching than Tyr residues. The 3D spectral analysis showed a relation of microenvironmental and conformational changes of Trp and Tyr residues in the peptide backbone, associated with the helix–coil transformation, which is confirmed by FT-IR studies. The present study can be useful to understand pharmacological and biochemical behavior of C1 and provide some valuable information for the quinoline scaffold design.

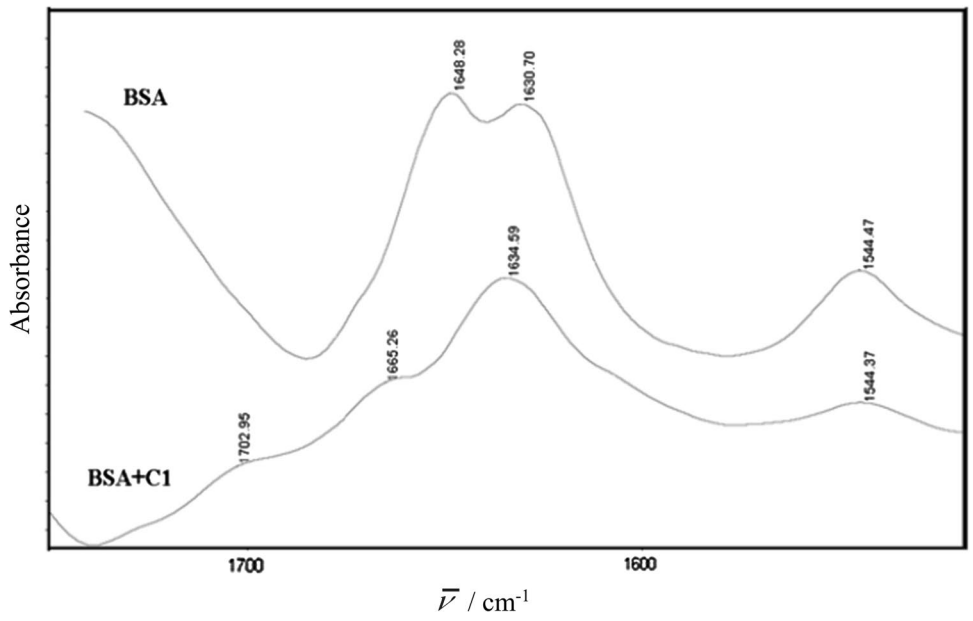

Fig. 8 Band-resolved FT-IR spectra of the amide I band of BSA and BSA–C1. $T = 298$ K, $(C1) = 6.0 \times 10^{-5}$ mol/dm^3

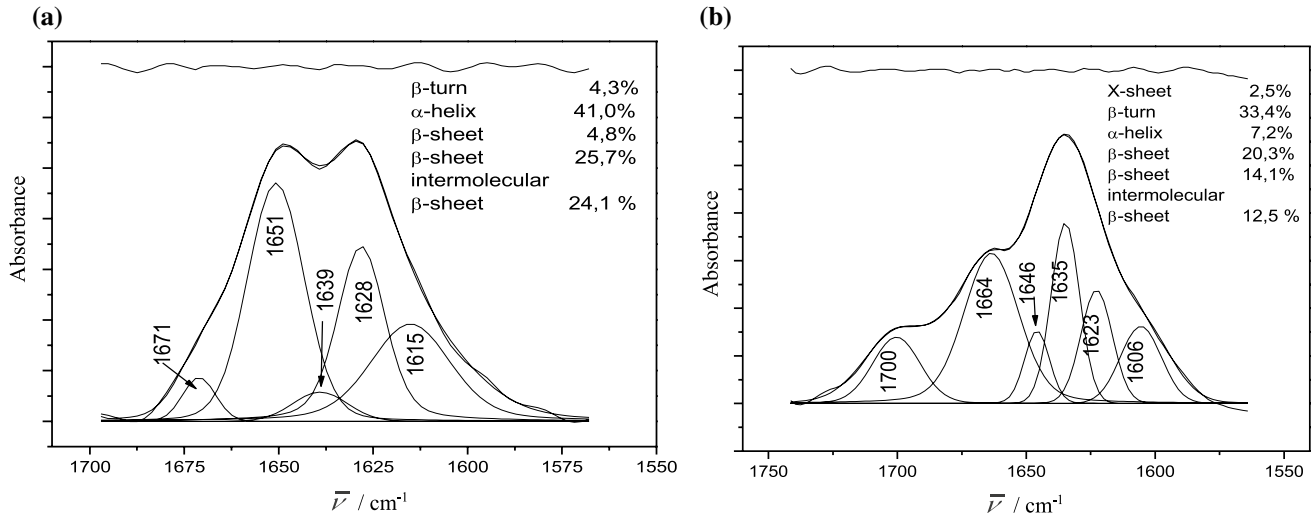

Fig. 9 Band-resolved FT-IR spectra of the amide I band of BSA (**a**) and BSA–C1 (**b**). $T = 293$ K, $(C1) = 6.0 \times 10^{-5}$ mol/dm^3

Experimental

C1 was synthesized and characterized according to [36]. Stock solution of C1 was prepared in dimethyl sulfoxide. Concentration of C1 was varied in the range of 1.00×10^{-5}–6.00×10^{-5} mol/dm^3. Bovine serum albumin (lyophilized) was purchased from the Sigma Chemical. Co. (USA) and used without further purification. Reagents used for the synthesis of C1 and for the preparation of solutions were of analytical grade. Concentration of BSA (0.4 mg/cm^3) was determined using UV/Vis spectra absorption at 280 nm with the extinction coefficient 4.3890×10^4 dm^3 mol^{-1} cm^{-1} [37]. BSA stock solution was prepared in saline solution.

Fluorescence spectroscopy studies

The fluorescence spectra were recorded on a Varian Cary Eclipse spectrofluorimeter (Australia), equipped with a temperature-controlled accessory. Measurements were carried out at 293, 298, and 303 K, in a range of $\lambda = 285$–500 nm at the excitation wavelength $\lambda = 280$ nm, using a quartz cell of 1 cm path length. The synchronous fluorescence spectra were recorded with scanning ranges $\Delta\lambda = 60$ and 15 nm in the absence of and in the presence of C1. The excitation and emission slits were set at 5 nm. The 3D fluorescence spectra were registered under the following conditions: excitation range ($\triangle\lambda_{ex}$) 200–450 nm, emission range ($\triangle\lambda_{em}$) 250–450 nm, $\lambda_{incr} = 10$ nm. The number of scans was 21. The excitation and emission slits were set at 5 nm. The

graphs and diagrams were constructed and analyzed, using the ORIGIN 8.5 software.

FT-IR spectroscopy studies

FT-IR spectra were recorded on a Nicolet/FT-IR NEXUS (USA) spectrometer using ATR attachment with a ZnSe crystal, in the range 4000–600 cm^{-1}, with a resolution of 4 cm^{-1} and number of scans 32. For the identification of the secondary structure and conformational changes of protein Gauss–Lorentz mixed function of the LinkFit program was used. The coexistence of different types of conformational and transformational species was confirmed by the analysis of observed peak frequencies. The peak frequency set was preliminary deduced by the second derivative method [38, 39]. Absolute error for BSA secondary structure FT-IR analysis is 1%.

Acknowledgements We are grateful to the Science Committee of the RA Ministry of Education, Science, Culture and Sports for financial support.

References

1. Harris CR, Thorarensen A (2004) Curr Med Chem 11:2213
2. Golden EB, Cho HY, Hofman FM, Louie SG, Schönthal AH, Chen TC (2015) Neurosurg Focus 38:E12
3. Sissi C, Palumbo M (2003) Curr Med Chem 3:439
4. Yadav DK, Rai R, Kumar N, Singh S, Misra S, Sharma P, Shaw P, Pérez-Sánchez H, Mancera RL, Choi EH, Kim M, Partap R (2016) Sci Rep 6:1
5. Jampilek J, Dolezal M, Kunes J, Vichova P, Jun D, Raich I, O'Connor R, Clynes M (2004) Curr Org Chem 8:1235
6. Ko TC, Hour MJ, Lien JC, Teng CM, Lee KH, Kuo SC, Huang LJ (2001) Bioorg Med Chem Lett 8:1235
7. Dermawan MD, Laitupa AA, Putra MA, Triastuti N (2020) J Qanun Medika 4:151
8. Musiol R (2017) Expert Opin Drug Discov 12:583
9. Guzman JD, Wube A, Evangelopoulos D, Gupta A, Hufner A, Basavannacharya C, Rahman M, Thomaschitz C, Bauer R, McHugh TD, Nobeli I, Prieto JM, Gibbons S, Bucar F, Bhakta S (2011) J Antimicrob Chemother 66:1766
10. Chu X, Wang C, Liu W, Liang L, Gong K, Zhao C, Sun K (2019) Eur J Med Chem 161:101
11. Kaur K, Jain M, Khan SI, Jacob MR, Tekwani BL, Singh S, Singh PP, Jai R (2011) Bioorg Med Chem 19:197
12. Macci F, Biver T (2021) J Inorg Chem 216:111305
13. Shilajyan HA, Grigoryan KR (2020) Monatsh Chem 151:135
14. Paul S, Roy P, Sardar PS, Majhi A (2019) ACS Omega 4:7213
15. Chakrabarty A, Mallick A, Haldar B, Das P, Chattopadhyay N (2007) Biomacromol 8:920
16. Peters T (1996) All about albumin. Biochemistry, genetics and medical application. Academic Press, San Diego
17. Peters T (1985) Adv Prot Chem 37:161
18. Lakowicz JR (2006) Principles of fluorescence spectroscopy, 3rd edn. Springer, New York
19. Grigoryan KR, Shilajyan HA, Aleksanyan IL, Grigoryan ZL, Hambardzumyan LP (2021) Proceed YSU 55:112
20. Nanda RK, Sarkar N, Banerjee R (2007) J Photochem Photobiol A Chem 192:152
21. Varlan A, Hillebrand M (2010) Molecules 15:3905
22. Koly SF, Kundu SP, Kabir S, Amran MS, Sultan MZ (2015) EPMA J 6:24
23. Grigoryan KR, Shilajyan HA, Hovhannisyan VA (2020) Proceed YSU 54:99
24. Van de Weert M, Stella L (2011) J Mol Struct 998:144
25. Ross P, Subramanian S (1981) Biochem 20:3096
26. Dresch JM, Liu X, Arnosti DN, Ay A (2010) BMC Syst Biol 4:142
27. Reshetnyak YK, Koshevnik Y, Burstein EA (2001) Biophys J 81:1735
28. Ghisaidoobe ABT, Chung S (2014) Int J Mol Sci 15:22518
29. Ranjbar S, Ghobadi S, Khodarahmi R, Nemati H (2012) Int J Biol Macromol 50:910
30. Bobone S, van de Weert M, Stella LA (2014) J Mol Struct 1077:68
31. Vishwas DS, Laxman SW, Anil HG, Prashant VA, Govind BK (2016) J Pharm Anal 6:56
32. Sandhya B, Ashwini HH, Ramesh KC, Seetharamappa J (2012) Spectrochim Acta Part A 86:410
33. Bortolotti AA, Wong YH, Korsholm SS, Hafizan N, Bahring B, Bobone S, Tayyab S, van de Weert M, Stella L (2016) RSC Adv 6:112870
34. Grigoryan KR, Zatikyan AL, Shilajyan HA (2021) J Biomol Struct Dyn 39:2284
35. Abrosimova KV, Shulenina OV, Paston SV (2016) J Phys Conf Ser 769:012016
36. Aleksanyan IL, Hambardzumyan LP (2019) Russ J Org Chem 55:262
37. Pace CN, Vajdos F, Fee L, Grimsley G, Gray T (1995) Protein Sci 4:2411
38. Murayama K, Tomida M (2004) Biochem 43:11526
39. Lorenz-Fonfria VA (2020) Chem Rev 120:3466